Supporting Information

Boosting Chem-insertion and Phys-adsorption in S/N co-doped Porous Carbon Nanospheres for High-performance Symmetric Li-ion Capacitors

Dong Yan[a,b,c], Jian Zhang[b], Dongbin Xiong[a,b], Shaozhuan Huang[b], Junping Hu[b], Mei Er Pam[b], Daliang Fang[b], Ye Wang[e], Yumeng Shi[a,d]*, Hui Ying Yang[b,c]*

[a]International Collaborative Laboratory of 2D Materials for Optoelectronics Science and Technology of Ministry of Education, Institute of Microscale Optoelectronics, Shenzhen University, Shenzhen 518060, China

[b]Pillar of Engineering Product Development, Singapore University of Technology and Design, 8 Somapah Road, 487372, Singapore

[c]Digital Manufacturing and Design Centre, Singapore University of Technology and Design, Singapore, 487372, Singapore

[d]Engineering Technology Research Center for 2D Material Information Function Devices and Systems of Guangdong Province, Institute of Microscale Optoelectronics, Shenzhen University, Shenzhen 518060, China

[e]Key Laboratory of Material Physics of Ministry of Education, School of Physics and Microelectronics, Zhengzhou University, Zhengzhou 450052, China

*Corresponding author E-mail: yumeng.shi@szu.edu.cn; yanghuiying@sutd.edu.sg

Experimental Section

Preparation of S/N co-doped porous carbon nanospheres

Typically, 1.95 g resorcinol and 1.95 g CTAB were added to a mixed solution including 1.95 mL ammonia, 195 mL deionized water and 78 mL ethanol with continues stirring for 30 min. Then, 9.75 mL TEOS and 2.73 mL formaldehyde solution were added into the above obtained solution with stirring for 24 h. Subsequently, the mixed solution was allowed to stand to form a white emulsion at room temperature. After that, the emulsion was centrifuged, then washed by water, and finally dried at 60 °C for 12 h. Next, the obtained sample was immersed in HF solution (10 wt.%) for 24 h at room temperature. After subsequent carbonizing, silicate was removed from the carbon-silicate sphere to form the N doped carbon spheres (NCS). Lastly, the SNCS were obtained by mixing the above powder and sublimed sulfur with a weight ratio of 1:1, and then realizing sulfidation at 500, 600 and 700 °C for 1 h under N_2 atmosphere.

Physical characterizations

Field emission scanning electron microscopy (FESEM, Hitachi S-4800), transmission electron microscopy (TEM, JEM-2010), X-ray photoelectron spectroscopy (XPS, Kratos Axis Ultra), X-ray diffraction (XRD, Bruker D8 Advance), Raman spectroscopy (Raman, Horiba T64000), Brunauer-Emmett-Teller (BET, ASAP 2046), and Barrett-Joyner-Halenda (BJH, ASAP 2046) were used to measure physical properties of all samples.

Computational Details

Density functional theory (DFT) was performed via employing plane wave

pseudopotentials with exchange-correlation of Perdew, Burke, and Ernzerhof (PBE) in Vienna ab initio simulation package (VASP). Besides, a plane-wave energy cutoff of 550 eV was used for all computations. In addition, Brillouin zone with Monkhorst-Pack k-point mesh of 3 × 3 × 1 is sampled for the structural optimization, and with the mesh of 5 × 5 × 1 for electronic structure calculation. Convergence criteria of ionic forces and total energy were set as 0.001 eV/Å and 10-4 eV, respectively. Besides, construction with a 18 Å vacuum zone at least in z direction was used to minimize the interactions in adjacent images. Meanwhile, DFT-D2 method in the all calculations was used due to the importance of van der Walls force in heteroatom anchoring materials.

Electrochemical characterizations

All electrodes were developed by mixing active materials (80 wt.%), super P (10 wt.%) and polyvinylidene fluoride (PVDF, 10 wt.%) in methyl-2-pyrrolidone (NMP) solution to form a slurry, and then casting obtained slurry onto Cu (anode) or Al (cathode) foils. All half-batteries were assembled in coin-type cells (CR2032) where prepared electrodes as working electrodes, Li metal as the counter electrodes, Celgard 2400 as separator, 1 M $LiPF_6$ in a solution of dimethyl carbonate (DMC) and ethylene carbonate (EC) (volume ratio of 1:1) as electrolyte. SLICs were also assembled in coin-type cells where prepared electrodes as both electrodes, Celgard 2400 as separator, 1 M $LiPF_6$ in a solution of DMC and EC as electrolyte. Besides, all anodes were pre-lithiated before assembling SLICs. The mass ratio of cathode and anode was experimentally fixed as 5:1 according to the charge equilibrium equation of $m_+C_+ = m_-C_-$ (C_+ and C_- are the specific capacity of cathode and anode; m_+ and m_- are the mass of cathode and anode

materials) [1]. The mass loadings of the cathode and anode active materials were controlled at ~ 10 mg (6.5 mg cm^{-2}) and 2 mg (1.3 mg cm^{-2}) in SLICs, respectively. Galvanostatic charge-discharge tests were performed on battery testing systems (LAND and Neware). Cyclic voltammetry (CV) curves were tested on the electrochemical workstations (Bio-Logic, VMP3; AUTO-LAB, PGSTAT302 N). Energy and power densities of LICs were obtained via employing the following equations:

$$\Delta V = (V_{max} + V_{min}) / 2 \quad (1)$$

$$P = \Delta V \times i/m \quad (2)$$

$$E = P \times t/3600 \quad (3)$$

where V_{max} is the beginning voltage value after the IR drop, and V_{min} is the end of discharge potentials (V), i is the current of discharge (A), t is the time of discharge process (s), m is the total mass of active materials in both anode and cathode (kg) [2].

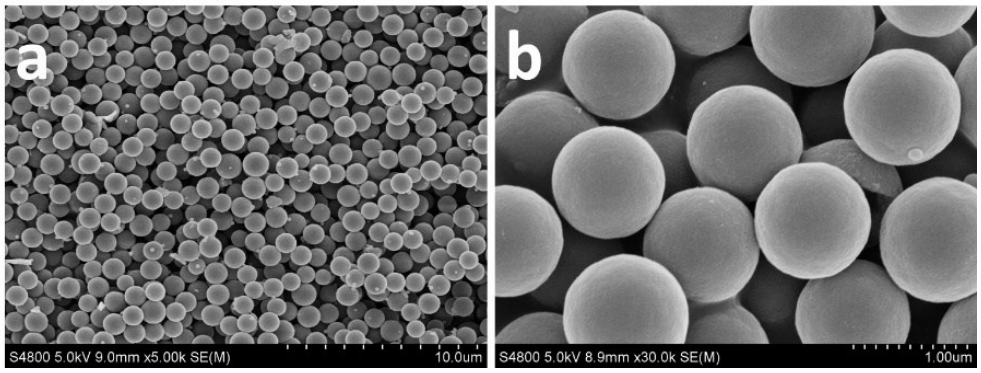

Fig. S1 FESEM images of carbon-silicate composite at different magnifications.

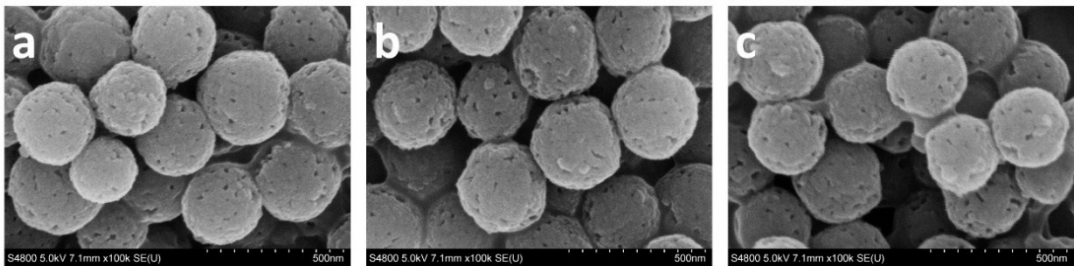

Fig. S2 FESEM images of NCS (a), SNCS-1 (b) and SNCS-3 (c).

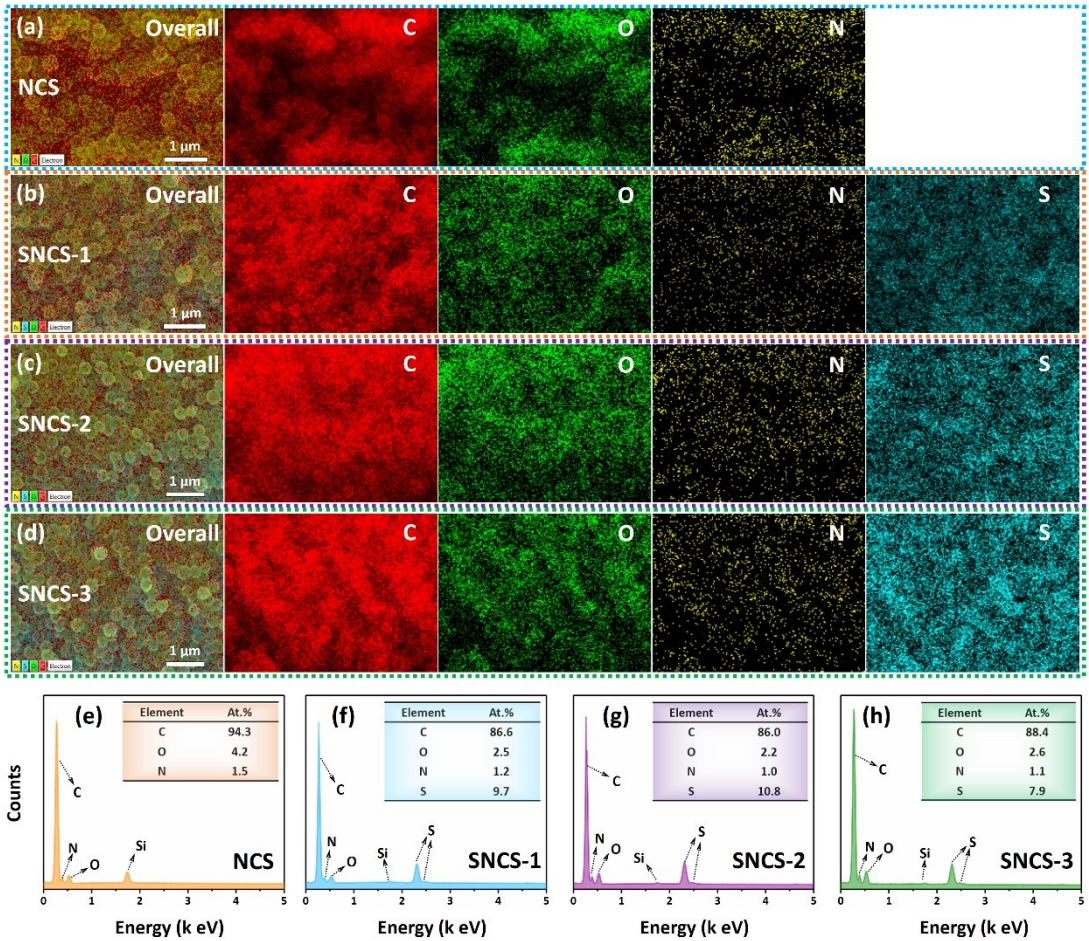

Fig. S3 EDS mapping images and corresponding EDS spectra of NCS (a, e), SNCS-1 (b, f), SNCS-2 (c, g), and SNCS-3 (d, h) on Si substrate.

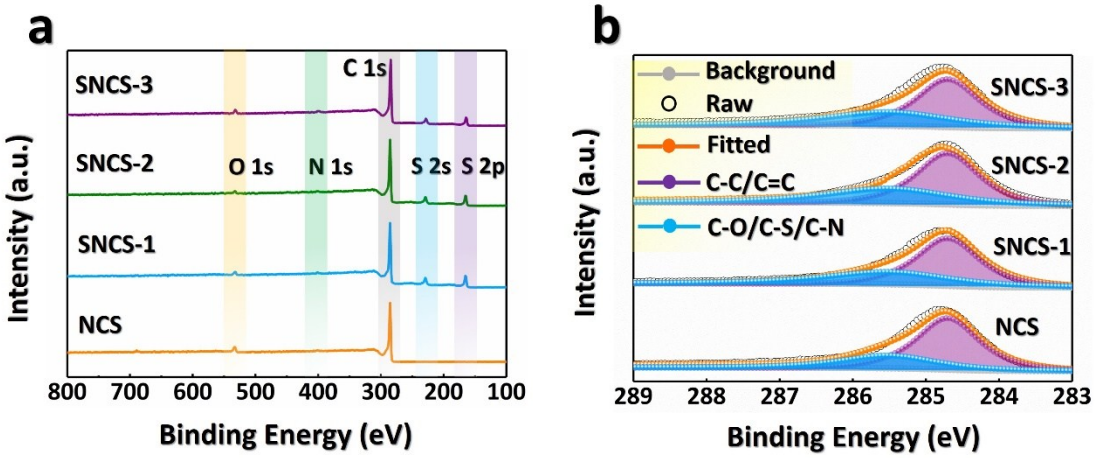

Fig. S4 XPS overall (a) and high-resolution C 1s (b) curves of NCS and SNCS.

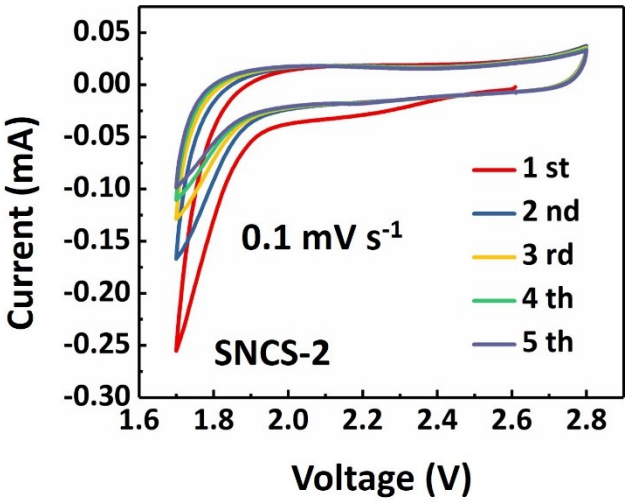

Fig. S5 CV curve of SNCS-2 as cathode for lithium-sulfur battery with voltage range of 1.7-2.8 V.

The Lithium-sulfur battery was assembled in coin-type cells (CR2032) where prepared SNCS-2 as cathode, Li metal as anode, Celgard 2400 as separator, 1 M bis(trifluoroethanesulfonyl) imide lithium (LiTFSI) in DME/DOL (v/v = 1:1) containing 0.3 M $LiNO_3$ as electrolyte. CV test was carried out by an electrochemical workstation (VMP3, Bio-Logic, Claix, France) at scan rate of 0.1 mV s^{-1}.

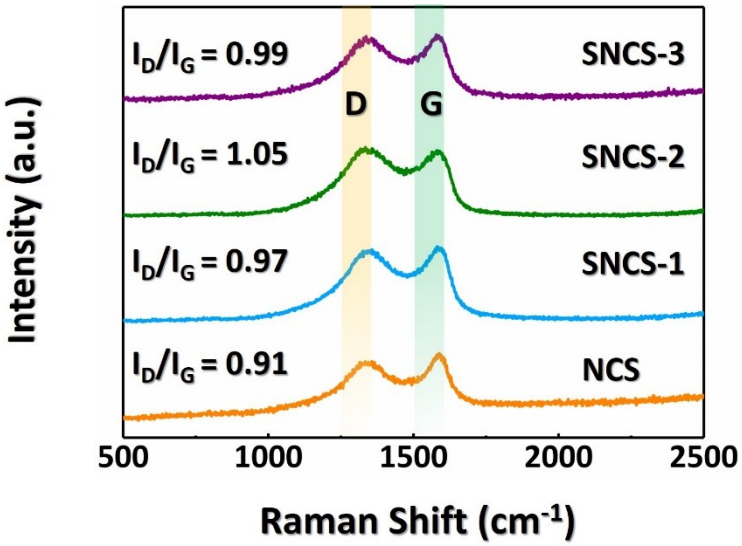

Fig. S6 Raman spectra of NCS, SNCS-1, SNCS-2 and SNCS-3.

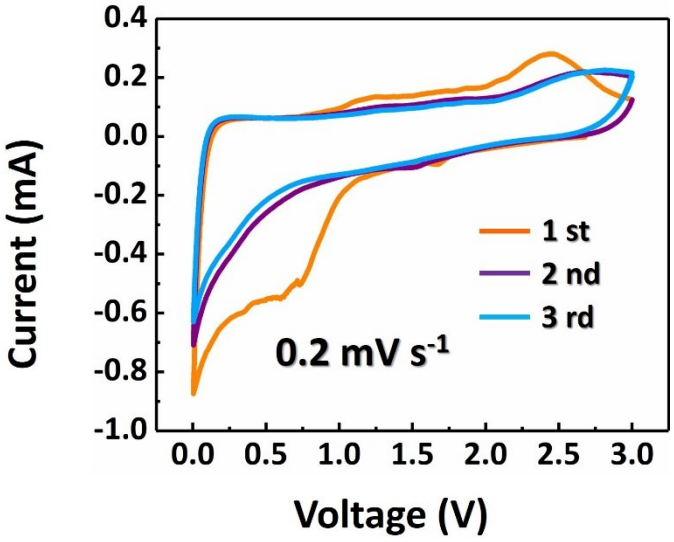

Fig. S7 CV curve of SNCS-2 at 0.2 mV s^{-1}.

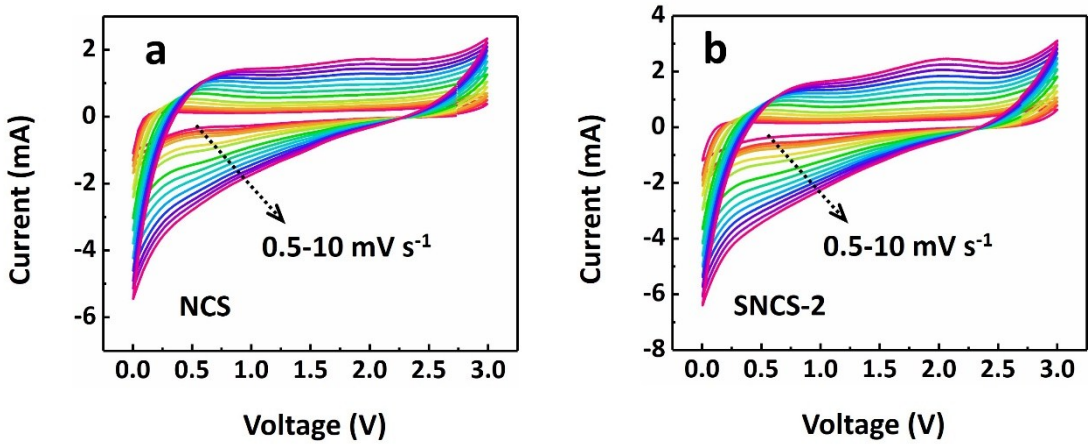

Fig. S8 CV curves of NCS (a) and SNCS-2 (b) at different scan rates.

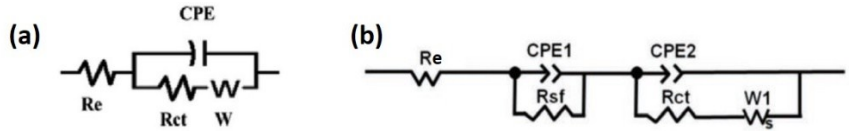

Fig. S9 Employed equivalent circuit in EIS study at OCV state (a) and after cycling (b).

EIS measurements of NCS and SNCS-2 were performed at OCV state and after 100 cycles, respectively. The Nyquist plots were further fitted according to the equivalent circuits (Fig. S9a and b), in which the R_e represent the resistance of the electrolyte, separator and electrode, R_{sf} reflect the resistance of SEI film, R_{ct} is charge transfer resistance, and W is the Warburg impedance [3]. It should be noted that the same separator, electrolyte and package were used to prepare the LIBs in this work. The difference of R_e and R_{ct} at OCV state can reflect the change of electrical conductivity and charge transfer at the electrolyte-electrode interfaces after S/N co-doping.

Moreover, the Li^+ diffusion coefficient (D_{Li}) could be calculated according to the formula of $D_{Li} = 0.5\frac{R^2T^2}{A^2n^4F^4C_{Li}^2\sigma^2}$. R is the gas constant, T represents the absolute temperature, A is the electrode area, n is the number of electrons transferred in the electrochemical redox reaction, F is the Faraday's constant, C_{Li} is the molar concentration of lithium ions in the solid, and the σ is the Warburg factor, which are determined from the slope of the Z_{re} - $\omega^{-1/2}$ lines (Fig. 3f) [4].

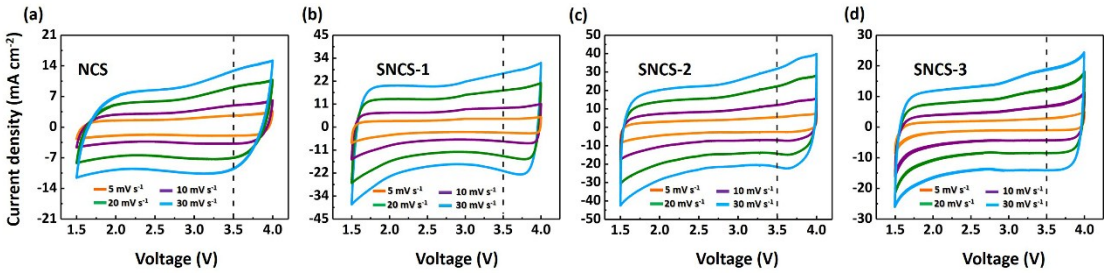

Fig. S10 CV curves of the NCS (a), SNCS-1 (b), SNCS-2 (c) and SNCS-3 (d) between 1.5 and 4 V at different scan rates.

To investigate the role of S/N co-doping on the electrochemical active surface areas (ECSA), the CV curves of NCS and SNCS were tested in the non-faradaic voltage range (1.5-4 V vs. Li/Li^+), as shown in Fig. S10. ECSA can be estimated based on the double-layer capacitance (Cdl), as the ECSA is generally proportional to its Cdl value [5]. Besides, Cdl can be calculated from the charging current density (i) and scan rate (v) according to the equation of Cdl = i/v [5], as seen in Fig. 5b.

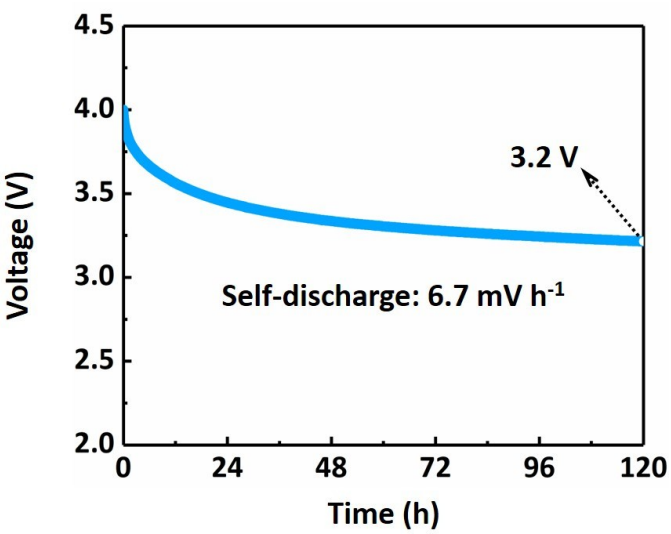

Fig. S11 Self-discharge behavior of the SNCS-2//SNCS-2 SLICs.

Table S1 Measured parameters from EIS spectra for NCS and SNCS.

Sample	R_e at OCV state (Ω)	R_{ct} at OCV state (Ω)	R_e after 100 cycle (Ω)	R_{sf} after 100 cycle (Ω)	R_{ct} after 100 cycle (Ω)	D_{Li} after 100 cycle ($cm^2 S^{-1}$)
NCS	3.44	397	4.81	29.8	798	4.95×10^{-13}
SNCS-2	2.67	305	3.01	14.1	412	8.57×10^{-13}

Table S2 Comparison of the electrochemical performances among SNCS-2 and other reported S/N co-doped carbons in LIBs, NIBs and KIBs.

Sample	Mass loading	Specific capacity at low current density	Rate performance	Long-term cycling Stability
SNCS-2 (This work)	2 mg	1100 mAh g^{-1} at 100 mA g^{-1} after 100 cycles	961 mAh g^{-1} at 200 mA g^{-1} 866 mAh g^{-1} at 500mA g^{-1} 750 mAh g^{-1} at 1A g^{-1} 564 mAh g^{-1} at 2 A g^{-1} 196 mAh g^{-1} at 5 A g^{-1}	Capacity retention of 82.3% after 500 cycles at 5 A g^{-1}
S/N co-doped carbon film in LIBs [6]	1.4 mg	880 mAh g^{-1} at 100 mA g^{-1} after 700 cycles	694 mAh g^{-1} at 200 mA g^{-1} 541 mAh g^{-1} at 500 mA g^{-1} 438 mAh g^{-1} at 1 A g^{-1} 347 mAh g^{-1} at 2 A g^{-1}	Capacity retention of 77% after 2000 cycles at 2 A g^{-1}
S/N co-doped carbon film in NIBs [6]	1.4 mg	403 mAh g^{-1} at 100 mA g^{-1} after 40 cycles	359 mAh g^{-1} at 200 mA g^{-1} 233 mAh g^{-1} at 500 mA g^{-1} 154 mAh g^{-1} at 1 A g^{-1} 92 mAh g^{-1} at 2 A g^{-1}	Capacity retention of 84% after 1000 cycles at 100 mA g^{-1}
S/N co-doped sisal carbon fiber in LIBs [7]	/	525 mAh g^{-1} at 50 mA g^{-1} after 50 cycles	~500 mAh g^{-1} at 100 mA g^{-1} ~420 mAh g^{-1} at 300 mA g^{-1} ~400 mAh g^{-1} at 500 mA g^{-1} 315 mAh g^{-1} at 1 A g^{-1} 246 mAh g^{-1} at 2 A g^{-1}	/
S/N co-doped porous carbon in LIBs [8]	1.15-1.44 mg	745 mAh g^{-1} at 100 mA g^{-1} after 100 cycles	849 mAh g^{-1} at 200 mA g^{-1} 676 mAh g^{-1} at 500 mA g^{-1} 569 mAh g^{-1} at 1 A g^{-1} 470 mAh g^{-1} at 2 A g^{-1} 426 mAh g^{-1} at 5 A g^{-1}	Capacity retention of ~50 % after 1000 cycles at 5 A g^{-1}
S/N co-doped Carbon sheet in LIBs [9]	3 mg	675mAh g^{-1} at 100 mA g^{-1} after 50 cycles	720 mAh g^{-1} at 100 mA g^{-1} 671 mAh g^{-1} at 250 mA g^{-1} 570 mAh g^{-1} at 500 mA g^{-1} 467 mAh g^{-1} at 1 A g^{-1}	/
S/N co-doped carbon sheet in NIBs [10]	/	350 mAh g^{-1} at 50 mA g^{-1} after 100 cycles	350 mAh g^{-1} at 50 mA g^{-1} 300 mAh g^{-1} at 100 mA g^{-1} 280 mAh g^{-1} at 200 mA g^{-1} 250 mAh g^{-1} at 500 mA g^{-1} 220 mAh g^{-1} at 1 A g^{-1} 190 mAh g^{-1} at 2 A g^{-1} 150 mAh g^{-1} at 5 A g^{-1} 110 mAh g^{-1} at 10 A g^{-1}	Capacity retention of ~100 % after 1000 cycles at 5 A g^{-1}

S/N co-doped carbon nanosheet in NIBs [11]	2 mg	/	371 mAh g^{-1} at 100 mA g^{-1} 322 mAh g^{-1} at 200 mA g^{-1} 286 mAh g^{-1} at 500 mA g^{-1} 247 mAh g^{-1} at 1 A g^{-1} 226 mAh g^{-1} at 2 A g^{-1} 212 mAh g^{-1} at 5 A g^{-1} 180 mAh g^{-1} at 10 A g^{-1}	Capacity retention of ~59.1 % after 1000 cycles at 1 A g^{-1}
S/N co-doped porous carbon sheet in KIBs [12]	/	254 mAh g^{-1} at 100 mA g^{-1} after 200 cycles	249 mAh g^{-1} at 50 mA g^{-1} 228 mAh g^{-1} at 100 mA g^{-1} 204 mAh g^{-1} at 200 mA g^{-1} 174 mAh g^{-1} at 500 mA g^{-1} 154 mAh g^{-1} at 1 A g^{-1} 135 mAh g^{-1} at 2 A g^{-1} 123 mAh g^{-1} at 3 A g^{-1}	Capacity retention of ~78.9 % after 2900 cycles at 1 A g^{-1}

Table S3 Comparison of the mass loading among SNCS-2 and other reported electrode materials in LICs.

Sample	Mass loading	Reference number in the manuscript
SNCS-2//SNCS-2 (This work)	2 mg//10 mg 1.3 mg cm^{-2}//6.5 mg cm^{-2}	/
$BiVO_4$//rGO [13]	1.6 mg//7.9 mg	[16]
MXene//activated carbon [14]	/	[17]
N doped carbon//N doped carbon [15]	1.2 mg cm^{-2}//3.6 mg cm^{-2}	[22]
$LiFePO_4$//activated carbon [16]	5 mg//14.6mg	[24]
Porous carbon//porous carbon [17]	/	[25]
N doped carbon//N doped carbon [18]	1 mg//3 mg	[28]
Carbon fiber//carbon fiber [19]	/	[29]
Si//carbon [1]	0.8-1 mg cm^{-2}//1.8-2 mg cm^{-2}	[63]
Nb_2O_5//carbon [20]	/	[64]
amorphous carbon//amorphous carbon [21]	0.7 mg//1.2 mg	[65]

References

[1] R. Shao, J. Niu, F. Zhu, M. Dou, Z. Zhang, F. Wang, Nano Energy, 63 (2019) 103824.

[2] A. Jagadale, X. Zhou, R. Xiong, D.P. Dubal, J. Xu, S. Yang, Energy Storage Mater., 19 (2019) 314.

[3] M. Si, D. Wang, R. Zhao, D. Pan, C. Zhang, C. Yu, X. Lu, H. Zhao, Y. Bai, Adv. Sci., 7 (2020) 1902538.

[4] L. Jin, R. Gong, W. Zhang, Y. Xiang, J. Zheng, Z. Xiang, C. Zhang, Y. Xia, J. P. Zheng, J. Mater. Chem. A, 7 (2019) 8234.

[5] J. Lin, Z. Zhong, H. Wang, X. Zheng, Y. Wang, J. Qi, J. Cao, W. Fei, Y. Huang, J. Feng, J. Power Sources, 407 (2018) 6.

[6] J. Ruan, T. Yuan, Y. Pang, S. Luo, C. Peng, J. Yang, S. Zheng, Carbon, 126 (2018) 9.

[7] D. Wang, K. Zhang, L. Liao, S. Chen, A. Qin, Int. J. Electrochem. Sci., 14 (2019) 102.

[8] H. Wan, X. Hu, Int. J. Hydrogen Energy, 44 (2019) 22250.

[9] G. Zhuang, J. Bai, X. Tao, J. Luo, X. Wang, Y. Gao, X. Zhong, X. Li, J. Wang, J. Mater. Chem. A, 3 (2015) 20244.

[10] J. Yang, X. Zhou, D. Wu, X. Zhao, Z. Zhou, Adv. Mater., 29 (2017) 1604108.

[11] D. Li, L. Chen, L. Chen, Q. Sun, M. Zhu, Y. Zhang, Y. Liu, Z. Liang, P. Sia, J. Lou, J. Feng, L. Ci, J. Power Sources, 41 (2019) 308.

[12] Y. Zhang, S. Tian, C. Yang, J. Nan, Dalton Trans., DOI: 10.1039/d0dt00697a.

[13] D.P. Dubal, K. Jayaramulu, R. Zboril, R.A. Fischer, P. Gomez-Romero, J. Mater. Chem. A, 6 (2018) 6096.

[14] P. Yu, G. Cao, S. Yi, X. Zhang, C. Li, X. Sun, K. Wang, Y. Ma, Nanoscale, 10 (2018) 5906.

[15] F. Sun, X. Liu, H.B. Wu, L. Wang, J. Gao, H. Li, Y. Lu, Nano Lett., 18 (2018) 3368.

[16] S. Jayaraman, S. Madhavi, V. Aravindan, J. Mater. Chem. A, 6 (2018) 3242.

[17] J. Niu, R. Shao, M. Liu, J. Liang, Z. Zhang, M. Dou, Y. Huang, F. Wang, Energy Storage Mater., 12 (2018) 145.

[18] T. Liang, H. Wang, R. Fei, R. Wang, B. He, Y. Gong, C. Yan, Nanoscale, 11 (2019) 20715.

[19] T. Le, H. Tian, J. Cheng, Z. Huang, F. Kang, Y. Yang, Carbon, 138 (2018) 325.

[20] X. Wang, P.S. Lee, J. Mater. Chem. A, 3 (2015) 21706.

[21] W.S.V. Lee, X. Huang, T.L. Tan, J.M. Xue, ACS Appl. Mater. Interfaces, 10 (2018) 1690.